New Journal of Physics
The open access journal at the forefront of physics

Deutsche Physikalische Gesellschaft DPG IOP Institute of Physics

PAPER • OPEN ACCESS

Unusual charge states and lattice sites of Fe in $Al_xGa_{1-x}N$:Mn

To cite this article: Hilary Masenda *et al* 2022 *New J. Phys.* **24** 103007

New Journal of Physics
The open access journal at the forefront of physics

Deutsche Physikalische Gesellschaft DPG
IOP Institute of Physics

Published in partnership with: Deutsche Physikalische Gesellschaft and the Institute of Physics

OPEN ACCESS

RECEIVED
28 April 2022

REVISED
17 September 2022

ACCEPTED FOR PUBLICATION
23 September 2022

PUBLISHED
7 October 2022

PAPER

Unusual charge states and lattice sites of Fe in $Al_xGa_{1-x}N$:Mn

Hilary Masenda[1,2,*], Haraldur Páll Gunnlaugsson[3], Rajdeep Adhikari[4], Krish Bharuth-Ram[5,6], Deena Naidoo[1], Aitana Tarazaga Martín-Luengo[4], Iraultza Unzueta[7], Roberto Mantovan[8], Torben Esmann Mølholt[9], Karl Johnston[9], Juliana Schell[9,10], Adeleh Mokhles Gerami[11], Petko Krastev[12], Bingcui Qi[3], Sveinn Ólafsson[3], Haflidi Pétur Gíslason[3], Arthur Ernst[13,14] and Alberta Bonanni[4]

[1] School of Physics, University of the Witwatersrand, Johannesburg, 2050, South Africa
[2] Faculty of Physics and Materials Sciences Center, Philipps-Universität Marburg, 35032 Marburg, Germany
[3] Science Institute, University of Iceland, 107 Reykjavík, Iceland
[4] Institute of Semiconductor and Solid State Physics, Johannes Kepler University, Altenbergerstrasse 69, A-4040 Linz, Austria
[5] Physics Department, Durban University of Technology, Durban 4000, South Africa
[6] School of Chemistry and Physics, University of KwaZulu-Natal, Durban 4001, South Africa
[7] Department of Applied Physics, School of Engineering Gipuzkoa, University of the Basque Country (UPV/EHU), Plaza Europa 1, 20018 San Sebastian, Spain
[8] CNR-IMM Unit of Agrate Brianza, Via Olivetti 2, 20864 Agrate Brianza (MB), Italy
[9] EP Dept, ISOLDE, CERN, 1211 Geneva 23, Switzerland
[10] Institute for Materials Science and Center for Nanointegration Duisburg-Essen (CENIDE), University of Duisburg-Essen, 45141 Essen, Germany
[11] School of Particles and Accelerators, Institute for Research in Fundamental Sciences (IPM), Tehran P.O. Box 19395-5531, Iran
[12] Institute for Nuclear Research and Nuclear Energy, Bulgarian Academy of Sciences, 1784 Sofia, Bulgaria
[13] Institute for Theoretical Physics, Johannes Kepler University Linz, Altenbergerstrasse 69, A-4040 Linz, Austria
[14] Max-Planck-Institut of Microstructure Physics, 06120 Halle, Germany
[*] Author to whom any correspondence should be addressed.

E-mail: hilary.masenda@wits.ac.za

Keywords: magnetic semiconductors, ion implantation, Mössbauer spectroscopy, density functional theory, exchange interactions

Abstract

Charge states and lattice sites of Fe ions in virgin and Mn-doped $Al_xGa_{1-x}N$ samples were investigated using ^{57}Fe emission Mössbauer spectroscopy following radioactive $^{57}Mn^+$ ion implantation at ISOLDE, CERN. In the undoped $Al_xGa_{1-x}N$, Fe^{2+} on Al/Ga sites associated with nitrogen vacancies and Fe^{3+} on substitutional Al/Ga sites are identified. With Mn doping, the contribution of Fe^{3+} is considerably reduced and replaced instead by a corresponding emergence of a single-line-like component consistent with Fe^{4+} on Al/Ga sites. Density functional theory calculations confirm the Fe^{4+} charge state as stabilised by the presence of substitutional Mn^{2+} in its vicinity. The completely filled spin up orbitals in Mn^{2+} ($3d^5$) are expected to enhance magnetic exchange interactions. The population of the Fe^{4+} state is less pronounced at high Al concentration in $Al_xGa_{1-x}N$:Mn, a behaviour attributable to hybridisation effects of 3d states to the semiconductor bands which weakens with increasing (decreasing) Al (Ga) content. Our results demonstrate that co-doping promotes the co-existence of unusual charge states of Fe^{4+} and Mn^{2+}, whereas their trivalent charge states prevail with either transition metal incorporated independently in III-nitrides. Co-doping thus opens up a new avenue for tailoring novel magnetic properties in doped semiconductors.

1. Introduction

III-nitrides and related alloys form a special class of semiconductors with extraordinary structural, optical, and electronic properties [1] which have earned them a wide range of applications in optoelectronic and high-frequency and high-power field-effect devices [2–5]. The usefulness of III-nitrides in these devices strongly rests on the ability to selectively dope the nitrides with foreign atoms, to realise p-type and n-type

conductivity, intentionally increase/decrease resistivity, or to tune intrinsic material properties via alloying [6]. Over the past decades, ion implantation has been a resourceful technique [7] for altering the structure of semiconducting materials thereby tuning the electronic, optical, and magnetic properties. Ion implantation offers control of dopant type, its depth profile and concentration, and by-passes thermodynamic solubility constraints in addition to allowing selective area doping [8]. Any implantation induced lattice damage, can be repaired by annealing or implantation at high temperatures. Successive to the ability to p-dope GaN with Mg [9–11] and the discovery of the blue LED [12–14], current research is focussed on improving performance of commercial devices made of III-nitrides and their alloys (ternary and quaternary) to broaden the range of applications because the capabilities of the material systems are yet to be fully explored. Recently, prospects for applications in water-splitting [15], photovoltaics [16], solar blind ultraviolet photodetectors [17] and deep ultraviolet lasers [18] have been reported. Moreover, for the past two decades, research interests have been focussed on efforts to realise dilute magnetism in group III-nitride semiconductors when doped with transition metals (TMs) targeting room temperature (RT) spintronic applications [19]. Among these are ternary semiconductors such as $Al_xGa_{1-x}N$, which are expected to give rise to unexpected photonic and magnetic functionalities when doped with TM ion species [20–22]. An understanding of the dopants' lattice sites, their local environments, associated defects and their nature in terms of charge and spin states is crucial, as these are linked to the inter-atomic bonding mechanisms thus influencing the resulting properties. In this letter, we present a study of the lattice locations and charge states of Fe ions in virgin and Mn (1 at %) doped $Al_xGa_{1-x}N$ using ^{57}Fe emission Mössbauer spectroscopy (eMS) for different Al concentrations (x). Mössbauer spectroscopy is a well-suited technique because of its sensitivity to the hyperfine interactions experienced by probe nuclei in a host material. The use of short-lived radioactive isotopes implanted in materials and Mössbauer spectroscopy presents a unique two-fold approach; (i) material modification by introducing the desired (daughter) dopant and (ii) characterisation at the atomic-scale of the local environment of the probe nucleus. Recently, this approach has been successfully applied to investigate lattice locations, charge states coupled with the nature and origin of magnetism in extremely dilute Fe implanted ZnO [23–25] and III-nitrides [26].

2. Experimental details

Radioactive $^{57}Mn^+$ ($t_{1/2}$ = 85.4 s) beams were produced at ISOLDE, CERN, following 1.4 GeV proton-induced nuclear fission in a heated uranium carbide (UC_2) target and selective multi-stage laser ionisation [27]. The singly charged ions were then accelerated to 50 keV energy and following magnetic mass separation yielded pure $^{57}Mn^+$ beams with intensities $\geqslant 10^8$ ions s^{-1}. Thin films of virgin $Al_xGa_{1-x}N$ (∼400 nm) and Mn (1 at %) doped $Al_xGa_{1-x}N$ (∼200 nm) were grown by metal–organic vapour phase epitaxy (MOVPE). Henceforth, these are also labelled as $Al_xGa_{1-x}N$ and $Al_xGa_{1-x}N$:Mn, respectively. Results emanating from comprehensive structural characterisation studies using different techniques are detailed in previous reports [20, 28, 29]. The samples were mounted on a magnet (B_{ext} = 0.6 T) inside an implantation chamber and held with the c-axis (0001) at 30° to the beam direction during implantation (θ_i). The diameter of the beam was ∼6 mm, and implantation fluences were kept below 3×10^{12} ions cm^{-2} to yield a concentration of $\sim 10^{-4}$ at %. SRIM [30] simulations show that the Mn (Fe) dopants in the nitride films are located within a depth 70 nm from the surface, (see appendix A). The eMS measurements were undertaken with a parallel plate avalanche counter (PPAC) equipped with ^{57}Fe enriched stainless steel and graphite electrodes. The PPAC was mounted on a conventional velocity drive unit located outside the implantation chamber at 90° relative to the beam direction as shown in figure 1. eMS data were acquired at RT on the 14.4 keV γ-rays from the ^{57}Fe Mössbauer state (populated from the ^{57}Mn β^- decay) at emission angle of $\theta_\gamma = 0°$ and 60° to the sample c-axis over a wide velocity scale of ±12 mm s^{-1}. For measurements at $\theta_\gamma = 0°$, the samples were first implanted for 180 s at 30° to the beam direction, then rotated to face the detector $\theta_\gamma = 0°$ and a new spectrum was recorded during the decay of $^{57}Mn^*$ for 240 s after the implantation. This process was repeated several times to obtain spectra with acceptable statistics. The isomer shift (δ) values and the velocity scale (inverted in comparison with conventional absorption Mössbauer spectroscopy) were calibrated relative to α-Fe at RT. The data analysis was carried out using the Vinda [31] code.

3. Results and discussion

The incorporation of Fe in binary III-nitrides has been studied both theoretically and experimentally [26, 32–43]. The lattice site, charge and spin states of intentionally introduced dopants determine the desired properties of materials. Fe^{3+} ($S = 5/2$) and Fe^{2+} ($S = 2$) are the most reported charge (spin) states

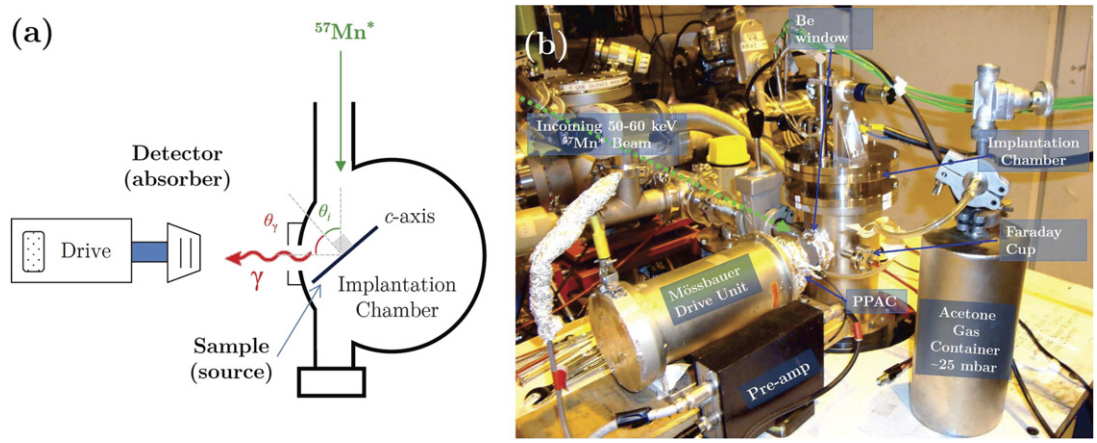

Figure 1. Arrangement of the sample, detector, and the ^{57}Mn* beam for the eMS experiments at ISOLDE, CERN: (a) schematic diagram and (b) pictorial top-view showing different components of the apparatus.

of Fe in AlN and GaN [26, 38]. RT emission Mössbauer spectra for $Al_{0.2}Ga_{0.8}N$ (for $x = 0.2$ or 20%) obtained at the two emission angles are shown in figure 2(a). The main features of the spectra are identical to those obtained for its binary counterparts, AlN and GaN [26], with a strong central component and spectral intensity in the wings of the spectra which exhibits the presence of slow relaxing paramagnetic Fe^{3+} [24] and was analysed with three sextets emanating from the three Kramers doublets belonging to the $S_Z = \pm 5/2, \pm 3/2, \pm 1/2$ crystal field states as depicted by a zoomed view in figure 2(c) resulting in the total magnetic contribution (Fe_{Mag}). This procedure is adopted from eMS studies of Fe in ZnO [23] where we first demonstrated that extremely dilute Fe in ZnO has a paramagnetic nature showing spin–lattice relaxation. The spin–lattice relaxation rates were further determined from the temperature dependence by monitoring the broadening of the sextets lines with increasing temperatures [24] using an empirical model described by Mølholt *et al* [44] based on the Blume–Tjon model [45]. The isomer-shift, $\delta = 0.12(1)$ mm s^{-1} and the maximum magnetic hyperfine field, $B_{hf} = 40(1)$ T are consistent with substitutional high-spin Fe^{3+} species observed in oxides and nitrides [23–26]. The magnetic features contribute 43(3)% to the spectral area. A quadrupole-shift $2\epsilon = -0.07(2)$ mm s^{-1} is extracted from the fitting, mainly determined by the prominent $S_Z = \pm 5/2$ state and applied for all other states. The hyperfine parameters of the three Kramers doublets do not match the expected parameters for high spin Fe^{3+} reported in Gütlich *et al* [46]. The reason for this is that the $B_{ext} = 0.6$ T is insufficient to 'unmix' the levels according to the splitting parameters from Heitz *et al* [47]; yet the observed behaviour is characteristic of paramagnetic Fe^{3+} as inferred from the previous studies [23–26].

The central region of the spectra was fitted with an asymmetric quadrupole split doublet in terms of Voigt line shapes. The two legs of the quadrupole split component possess different widths allowing for coupling between the isomer shift and the quadrupole splitting. The relative intensities were allowed to account for the possible angular dependence as discussed in Masenda *et al* [26] expected on a regular lattice site in a wurtzite crystals. The experimental lineshape obtained from implantation into iron foils was best described using a Voigt profile with Lorentzian broadening of 0.34 mm s^{-1} and Gaussian broadening of 0.1 mm s^{-1}. The observed angular dependence is indicative of Fe atoms in crystalline environments (Fe_C), occupying the remaining 57(3)% of the spectral area. The hyperfine parameters of the doublet were determined as $\delta = 0.58(1)$ mm s^{-1} and the average quadrupole splitting $\Delta E_Q = 1.48(1)$ mm s^{-1} at RT. The isomer shift value is close to the one expected for dilute high-spin Fe^{2+} ($\delta = 0.47$ mm s^{-1}) estimated using the semi-empirical model developed by Gunnlaugsson and Masenda [48] from 22 compounds with δ values showing a standard deviation of ± 0.1 mm s^{-1}. The model takes into account nearest neighbour distances and electronegativity of the hosts and allows the assignment of this component to substitutional Fe^{2+}. The obvious donor defects that would promote the Fe^{2+} charge state above the natural Fe^{3+} charge state are nitrogen vacancies (V_N) created during the ion implantation process [26]. Our data show no evidence of low intensity components (due to interstitial Fe), nor angle-independent broadened components characteristic of Fe atoms in implantation induced amorphous zones. This is consistent with previous eMS studies on similar semiconductors employing radioactive probes with extremely dilute implantation fluences, where amorphization like defects are excluded [25].

To study the effects of Mn-doping, eMS measurements were undertaken on ternary samples pre-doped during MOVPE growth with Mn to concentrations of 1 at % ($Al_xGa_{1-x}N$:Mn). The RT spectra for

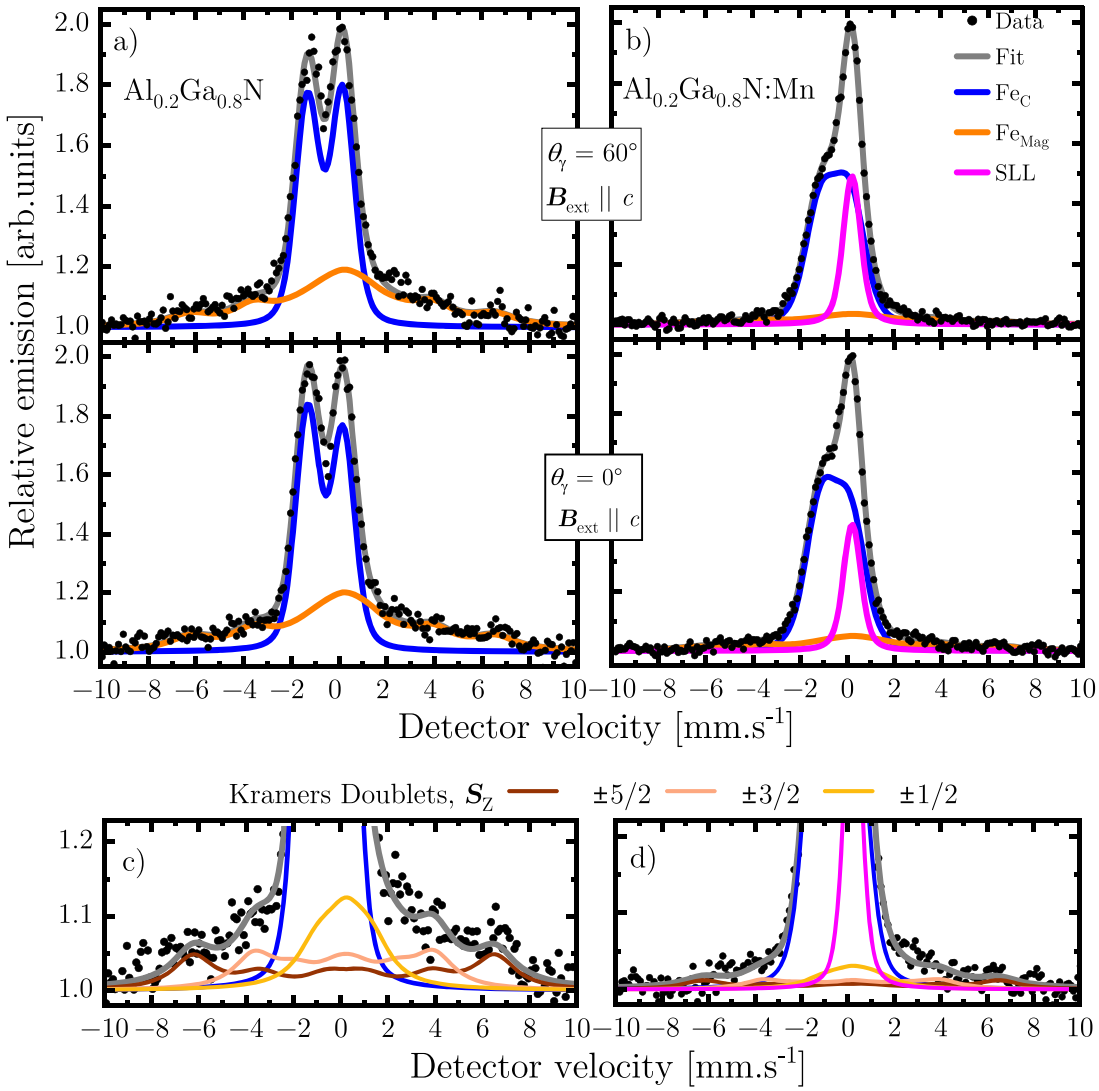

Figure 2. RT ^{57}Fe emission Mössbauer spectra obtained at emission angles of 0° (bottom) and 60° (top) following implantation of $^{57}Mn^*$ into (a) $Al_xGa_{1-x}N$ and (b) $Al_xGa_{1-x}N$:Mn for $x = 20\%$ (0.2) in an external magnetic field, $B_{ext} = 0.6$ T. The bottom panels, (c) and (d) illustrate zoomed views showing individual contributions from the $S_Z = \pm 5/2, \pm 3/2, \pm 1/2$ crystal field states to Fe_{Mag} for respective spectra measured at $\theta_\gamma = 0°$.

$Al_{0.2}Ga_{0.8}N$:Mn at emission angles of 0° and 60° are shown in figure 2(b). Identical fitting components as utilised in the undoped alloys ($Al_xGa_{1-x}N$) were employed. However an additional single-line-like (SLL) component was required to obtain reasonable fits to the data. The SLL is characterised by an $\delta = -0.22(1)$ mm s^{-1} and contributes approximately 24(3)% to the spectral area. An additional Gaussian broadening of the SLL by $\simeq$0.27(2) mm s^{-1} suggests the presence of a minor unresolved quadrupole interaction expected for an Fe atom on a substitutional cation site in III-nitrides. Fe^{2+} still dominates the spectra with 63(3)% but the Fe^{3+} contribution is significantly reduced to 13(2)%. As depicted in figure 2(b). The values of the hyperfine parameters of the Fe^{2+} doublet are slightly lower in Mn doped AlGaN and were determined as $\delta = 0.49(1)$ mm s^{-1} and $\Delta E_Q = 1.25(1)$ mm s^{-1}. Thus confirming the shrinking effect of the lattice in the neighbourhood of the probe atoms due to a smaller Mn occupying a relatively larger substitutional Ga site. These values are still consistent with a substitutional high-spin Fe^{2+} with V_N in its vicinity. The smaller δ corresponds to an increase in the s-electron density at the probe nucleus, indicative of increase of the bonding strength between the Fe ions and the surrounding lattice atoms. The lower ΔE_Q, suggests less distorted local environment (from tetrahedral symmetry) around the Fe probe atoms in AlGaN:Mn. The centre of the $S_Z = \pm 1/2$ appears to coincide with the position of the SLL and enhanced in the presence of an external magnetic field, see figures 2(c) and (d). The narrow splitting of the $S_Z = \pm 1/2$ in high magnetic field is consistent with observation reported in dilute frozen solutions [49, 50]. This effect is confirmed by spectra obtained for $Al_{0.2}Ga_{0.8}N$ and $Al_{0.2}Ga_{0.8}N$:Mn without an external magnetic field ($B_{ext} = 0$ T) shown in figures 3(a) and (b). The focussed in views of the respective spectra in figures 3(c) and (d) clearly demonstrate the effects of an external magnetic field on the $S_Z = \pm 1/2$. Moreover, this affirms the presence

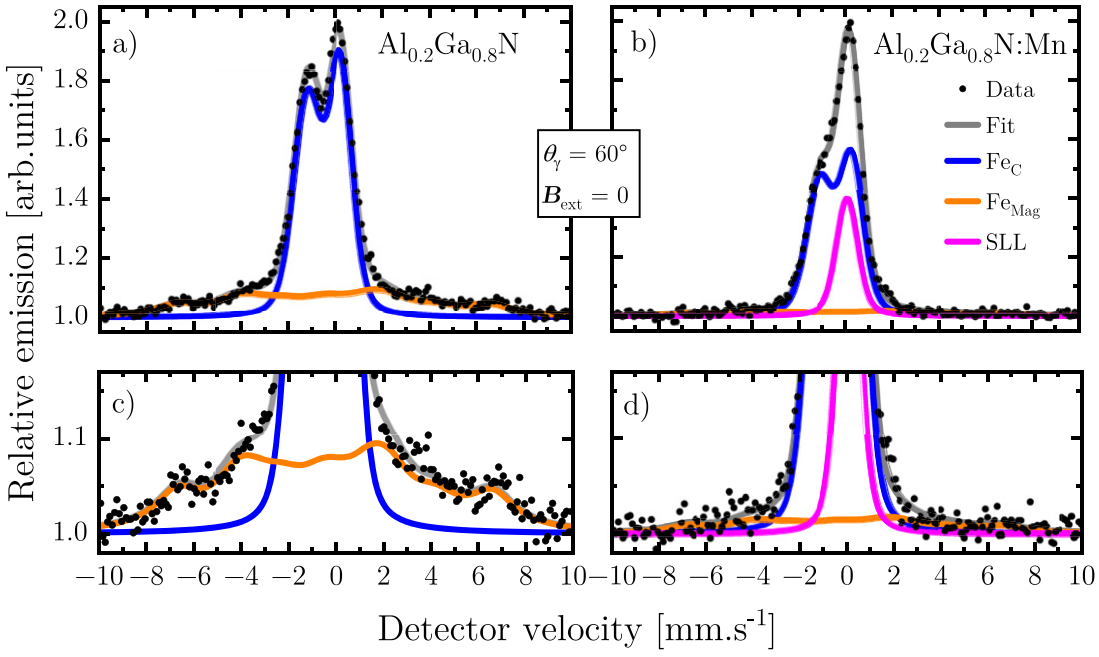

Figure 3. RT ^{57}Fe emission Mössbauer spectra obtained at emission angles of 60° after implantation of ^{57}Mn* into (a) $Al_xGa_{1-x}N$ and (b) $Al_xGa_{1-x}N$:Mn for $x = 20\%$ (0.2) without an external magnetic field ($B_{ext} = 0$ T), (c) and (d) are zoomed views showing the Fe_{Mag} contributions for respective spectra.

of the SLL component in Mn doped $Al_{0.2}Ga_{0.8}N$ which is coupled with a significant reduction in the magnetic contribution.

An obvious assignment of the SLL could be due to interstitial Fe. However, recoil produced interstitials were not observed in undoped $Al_xGa_{1-x}N$ samples and in similar experiments on binary nitrides [26]. These Fe interstitials were evident in cubic III–Vs such as GaAs and GaP [51] as minor components at low temperatures, with an isomer shift, $\delta \simeq 1$ mm s^{-1}. Transmission and conversion electron Mössbauer studies [32, 35, 37, 52] of Fe in GaN and AlN after relatively high fluences (10^{16-17} ion cm^{-2}) show the presence of a single line with comparable isomer shift values. The single line was assigned to Fe precipitates (either superparamagnetic α-Fe or paramagnetic γ-Fe). The dilute Fe concentration employed in the eMS experiments described here, excludes the probability of forming such precipitates. In our previous fluence-dependent studies on Fe pre-implanted ZnO [25] with effective Fe concentrations up to 2.2 at %, onset of spin–spin interaction is evident at 0.02 at %. Such precipitates are expected at the upper threshold. On the other hand, emission chanelling (EC) studies showed ∼20% anion site substitution in Mn-implanted GaN [53], (∼27%) and (∼18%) anion site substitutions, in Mn- and Co-implanted ZnO, respectively [54]. However, a similar anion site occupation has not been observed in the EC studies on the Fe-implanted GaN [33] and ZnO [55]. This agrees with the eMS studies on GaN and AlN using ^{57}Mn* [26]. Significant differences in the lattice locations are not expected since Mn, Fe and Co have comparable atomic radii and masses. Therefore, it is intriguing that anion site substitution of Mn (and Co) is favoured, considering the Fe properties (size and electronegativity) are intermediary. More so, in eMS using radioactive ^{57}Mn, where the daughter (^{57}Fe) inherits lattice location from the parent ^{57}Mn site after β^- decay. Nonetheless, this can be explained by the recent theoretical studies [43, 56] which report very high formation energies for anion site occupation of Fe in binary nitrides. This stems from ionic radii mismatch between Fe and N atoms. Thus, a positively charged Fe on a N site will be thermodynamically unstable. This further excludes the probability to assign the SLL component we observed in eMS to the anion site occupation, and promotes us to suggest that this component is due to Fe atoms on substitutional Ga/Al sites. Wickramaratne *et al* [43] found the 4+ state to be stable in both GaN and AlN, with a (4+/3+) level at 0.26 eV and 0.36 eV, respectively, above the valence band maximum. Consequently, in light of the above discussions and based on the extracted isomer shift value, a plausible interpretation for the SLL is Fe^{4+} on Ga/Al sites based on the isomer shift reference scale given by Gütlich *et al* [46].

To gain insights into the nature of the observed charge states, measurements were performed for different Al concentration (x) at RT. Additional representative spectra for both $Al_xGa_{1-x}N$ and $Al_xGa_{1-x}N$:Mn are included in appendix B. More importantly, the extracted relative area contributions of different charge states (fitted components) as a function of Al content are presented in figure 4. The

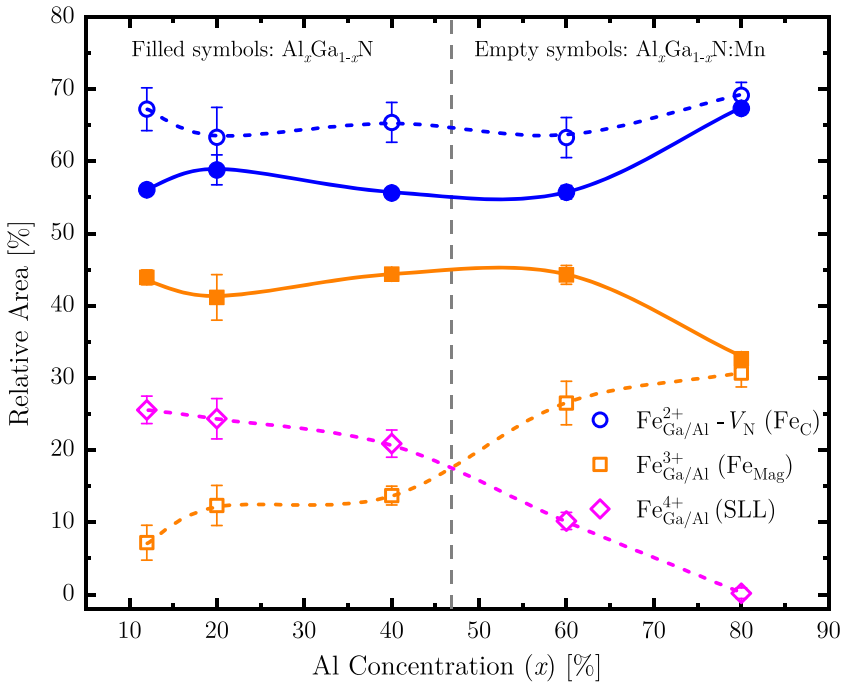

Figure 4. Relative area fractions at RT as a function of concentration (x) for $Al_xGa_{1-x}N$ (filled symbols) and $Al_xGa_{1-x}N$:Mn (empty symbols). The solid and dashed lines are guides to the eye.

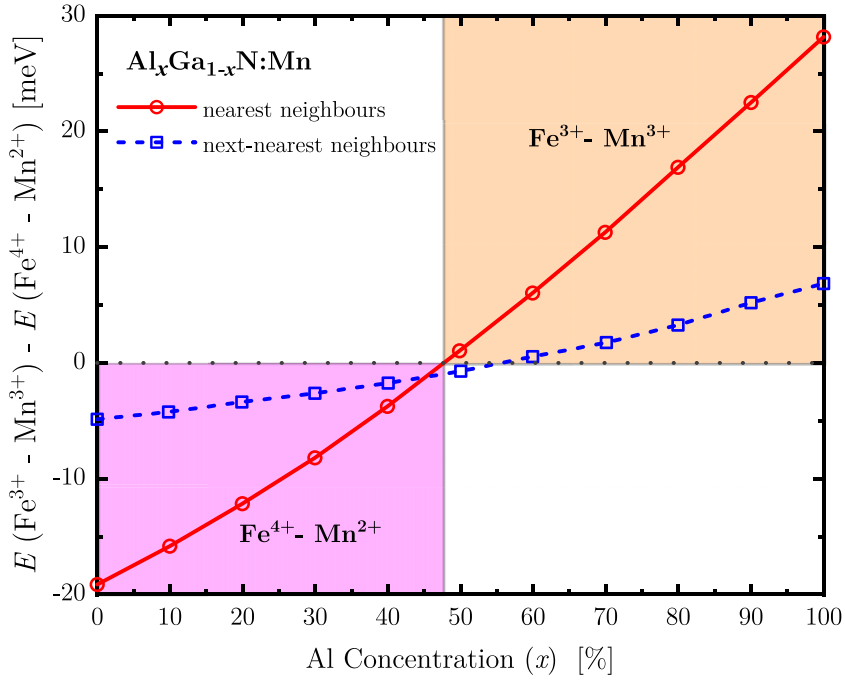

Figure 5. Formation energy difference between Fe^{3+}–Mn^{3+} and Fe^{4+}–Mn^{2+} configuration as a function of x in $Al_xGa_{1-x}N$:Mn. Solid (dashed) lines show the energy difference when Fe and Mn are nearest (next nearest) neighbours while the shaded areas show regions of stability for the corresponding configurations.

concentration of Fe^{2+} is fairly stable, while a decrease in the proposed Fe^{4+} (SLL) state (detected only in the AlGaN:Mn samples) is accompanied by an increase in the Fe^{3+} state. This suggests that an increase in Al content suppresses the formation of the Fe^{4+}, thereby maintaining an iso-electronic charge state.

A deeper understanding of the mechanism favouring the 4+ state is needed to confirm its nature. In this pursuit, first-principles calculations were carried using a multiple-scattering Green's function method designed for bulks, surfaces, interfaces and embedded clusters [57]. The calculations were carried out within the density functional theory (DFT) in a local density approximation [58] (see appendix C for extra

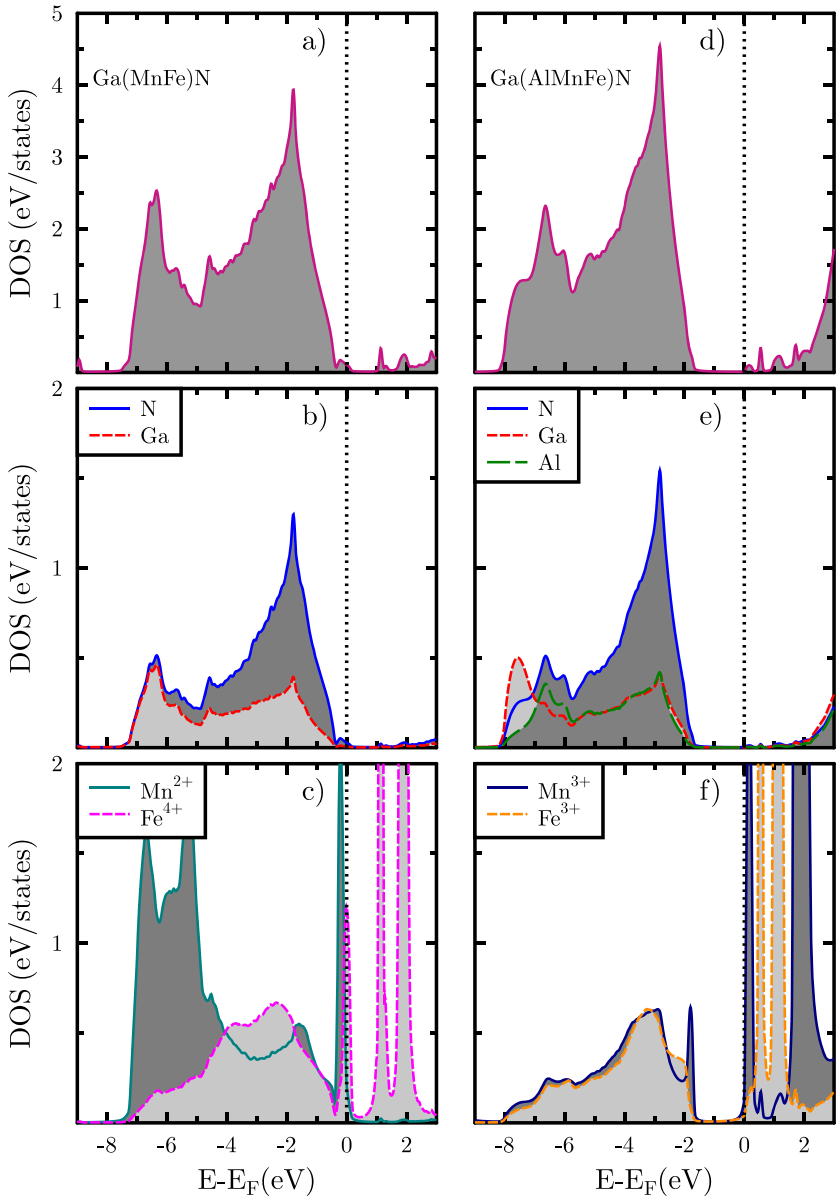

Figure 6. DOS for: Ga(MnFe)N (a)–(c) and Ga(AlMnFe)N (d)–(f) calculated assuming Fe^{4+}–Mn^{2+} scenario for Ga(MnFe)N and Fe^{3+}–Mn^{3+}—for Ga(AlMnFe)N cases: (a) the total DOS of Ga(MnFe)N; (b) atomic resolved DOS for Ga and N in Ga(MnFe)N; (c) atomic resolved DOS for Mn^{2+} and Fe^{4+} in Ga(MnFe)N; (d) total DOS of Ga(AlMnFe)N; (e) atomic resolved DOS for Ga, Al and N in Ga(AlMnFe)N; (f) atomic resolved DOS for Mn^{3+} and Fe^{3+} in Ga(AlMnFe)N.

details). Strongly localised Mn 3d electrons were treated using a self interaction correction (SIC) method [59] as it is implemented within the multiple-scattering theory [60]. This approach provides an adequate description of ground state properties of diluted magnetic semiconductors doped with TM elements [61]. Especially, the method predicts correctly the valency of TMs in III–V semiconductors [61]. To determine the valency, the total energy of various configurations of 3d electrons treated with the self interaction are compared. In particular, Mn in GaN was found to be trivalent, Mn^{3+} (d^4). Considering the given problem it needs to proven whether the presence of Al and Mn–Fe hybridisation might change the valency of both Mn and Fe ions. In this regard, we performed the calculations in two steps. First, $Al_xGa_{1-x}N$ doped with 2% of Mn^{3+} was calculated for various x in its bulk structure using a coherent potential approximation (CPA) as it is implemented within the multiple scattering theory [62, 63]. Then, Mn and Fe impurities were embedded into the (AlGaMn)N effective medium in real space representation. Thereby, various combinations of valencies and structural configurations of the two TMs (Mn and Fe) in close proximity could be considered as the result from substitutional incorporations of (a) Fe^{3+}–Mn^{3+}, (b) Fe^{4+}–Mn^{2+} and/or (c) interstitial–substitutional configuration of Fe^{4+}–Mn^{2+}. In light of the earlier discussion, the (c) configuration can be excluded since neither as-grown Mn nor parent (daughter) $^{57}Mn^*$ (^{57}Fe) prefers interstitial occupations. A total energy comparison provides the preferable valencies of Mn and Fe ions for a

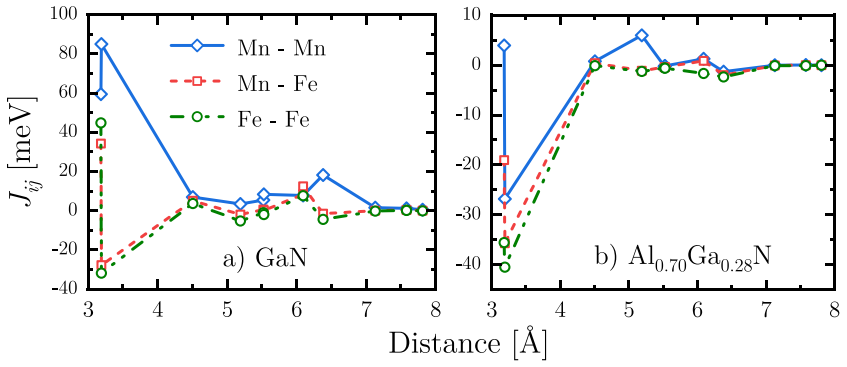

Figure 7. Interatomic exchange interaction parameters, J_{ij} of TM atoms i and j in (a) GaN and (b) AlGaN.

given Al concentration and a given geometry. The total energy difference (ΔE) between the formation energies of Fe^{3+}–Mn^{3+} and Fe^{4+}–Mn^{2+} as a function of Al concentration is presented in figure 5.

The negative ΔE at low Al concentrations attests that the Fe^{4+}–Mn^{2+} configuration is the most likely candidate. On the other hand, the Fe^{3+}–Mn^{3+} is energetically favourable by ∼14 eV [64] for the combination of isolated charge state configurations. This confirms that the local environment, especially the relative amounts of Al/Ga play a crucial role on the stability of different charge state configurations in the material system. In addition, the large negative ΔE at low Al composition indicates that the Mn ions in very close vicinity to the probe atom (solid curve) are more likely to favour the 4+ charge state compared to Mn as next nearest neighbours (dashed curve). Furthermore, for the nearest neighbours case; the $Fe^{4+} \rightarrow Fe^{3+}$ transition *climax* extracted from the experimental data (figure 4—dashed vertical line) occurs at Al concentration of $x \sim 47\%$, this coincides perfectly with the switch in stability (i.e. at $\Delta E = 0$) between Fe^{4+}–Mn^{2+} and Fe^{3+}–Mn^{3+} configurations (shaded regions in figure 5). This compositional dependence is explained by the increased hybridisation 3d states in Al rich alloys as the inter-atomic distances of Ga decreases. The effect of Al concentration on the charge state of Fe–Mn is attributed to hybridisation effects. This can be understood in that Ga valence states are sufficiently broad in energy when compared with Al and, therefore, they hybridise strongly with 3d states of TMs. Figure 6 displays the detailed density of states calculated utilising the SIC approach. Due to the strong hybridisation, the localisation of 3d states is expected to be reduced. Since the densities of states (DOS) of Fe 3d states are higher than that of Mn 3d states, the Fe 3d states hybridise with the Ga valence bands more strongly than the Mn 3d states (figures 6(a)–(c)).

However, in the absence of Mn, Fe is still in the 3+ charge state because of the charge neutrality condition. Thus, the iso-electronic substitution takes precedence. On the other hand, with doping, Mn can easily localise one more electron, Fe becomes 4+; the Mn 3d states are lower in energy and, therefore, are weakly bound on the semiconductor bands. Thus, Mn becomes 2+ in the presence of Fe 4+ to make the system charge neutral. In this case, all five Mn 3d spin up states are occupied and localised. This depends on the concentration of Al; with increase of Al content, the Ga content reduces and, therefore, the hybridisation with Ga 3d states weakens (figures 6(d)–(f)). Consequently, with all spin up 3d states occupied, the presence of Mn^{2+} is envisaged to increase considerably the magnetic exchange interaction in the system. This is evident in figure 7 which shows the differences in the interatomic exchange parameters, J_{ij}, which represent the magnetic interaction between magnetic moments of TM atoms i and j in (a) GaN and (b) AlGaN.

The concentrations of Mn and Fe were set to 1 at %, Al at 70% and the remainder to Ga. In the case of Fe, the 1 at % is selected to observe a sizeable effect in the calculations; whereas in the experiment, fluences are in the extremely dilute regime (10^{-4} at %). The most significant exchange interaction is observed for the Mn–Mn case. Whereas the Mn^{3+}–Mn^{3+} exchange parameters in AlGaN indicate a frustrated magnetic order (the nearest and the next nearest J's have opposite sign), the magnetic interaction between Mn^{2+} moments in GaN is larger in magnitude and overall positive favouring a stable ferromagnetic order. These results are consistent with previous studies [65], where the presence of Mn^{2+} in GaN was assumed. Furthermore, the Mn^{2+} state has been observed in different dilute magnetic semiconducting materials such as (Ga, Mn)As [66] and (BaK)$(ZnMn)_2As_2$ [67, 68] of the so-called '122 type'. It should be re-iterated here that under normal conditions (i.e. without Fe) Mn has the valency 3+ in GaN. The same is true for Fe, in the absence of Mn, the 3+ state is adopted. Thus, doping with both Fe and Mn atoms in GaN promotes the co-existence of unusual charge states of Fe^{4+} and Mn^{2+}, as observed from

eMS experiments; which is mainly sensitive to Fe^{4+} state is while DFT calculations confirm and identify Mn^{2+} as its nearest neighbour.

4. Conclusions

Briefly, the Mössbauer spectra of ^{57}Fe incorporated in $Al_xGa_{1-x}N$ show the presence of magnetically-split sextets extending to the 'wings' of the spectra, which on the basis of our earlier studies are attributed Fe^{3+} on Al/Ga sites ($Fe^{3+}_{Al/Ga}$). The central part of the spectra represent the paramagnetic Fe^{2+} on Al/Ga sites associated with nitrogen vacancies ($Fe^{2+}_{Al/Ga}$–V_N). However, with Mn doping, the contribution of Fe^{3+} is reduced substantially accompanied by the appearance of a single line component with Mössbauer parameters characteristic of Fe^{4+} on Al/Ga sites ($Fe^{4+}_{Al/Ga}$), which is stabilised by the presence of Mn^{2+} as nearest neighbours. These unusual charge states and structural configuration (in III-nitrides) are confirmed by DFT calculations. Moreover, the 4+ charge state is suppressed at higher Al concentrations and this is attributed to the weakened hybridisation of the Mn 3d states with the Ga valency states with increasing Al content. Our results demonstrate the co-existence of Fe^{4+} and Mn^{2+} unusual charge states in Fe and Mn co-doped ternary nitrides, indicating the presence of an extra acceptor level and/or enhanced magnetic exchange interactions between the doped TM atoms. These results offer insights into understanding the dilute magnetism in nitride semiconductors via co-doping with TMs as an alternative approach. The material system offers prospects for applications in spintronic and/or optoelectronic devices.

Acknowledgments

This work was supported by the European Union Seventh Framework through ENSAR (Contract No. 262010) and the German BMBF under Contract Nos. 05K13TSA and 05K16PGA. The work was funded by the Austrian Science Fund (FWF) through Projects No. P26830 and No. P31423. H Masenda, K Bharuth-Ram, and D Naidoo acknowledge support from the South African National Research Foundation and the Department of Science and Innovation within the SA-CERN programme. H Masenda also acknowledges support from the Alexander von Humboldt (AvH) Foundation. B Qi, H P Gíslason and S Ólafsson acknowledge support from the Icelandic Research Fund. I Unzueta thanks the support of (MINECO/FEDER) and the Basque Government for the Grants RTI2018-094683-B-C5 (4, 5) and IT-1005-16, respectively.

Data availability statement

The data that support the findings of this study are available upon reasonable request from the authors.

Conflict of interest

The authors have no conflicts to disclose.

Appendix A. Implantation profiles: SRIM/TRIM simulations

The thicknesses of MOVPE grown $Al_xGa_{1-x}N$ and $Al_xGa_{1-x}N$:Mn samples were ∼400 nm and 200 nm, respectively. Depth profiles are commonly simulated using TRIM which employs a Monte-Carlo method [30] to ascertain the projected range of implanted impurity ions. To investigate the implantation range of ^{57}Mn (^{57}Fe) ions in the ternary alloy of $Al_xGa_{1-x}N$ its binary counterparts were employed to set limits. Figure A1 represent simulated for AlN and GaN matching experimental implantation details of 50 keV at an implantation angle of 30° using 10^6 ions to acquire good statistics.

The resulting Gaussian-like implantation profiles have peak concentrations at an implantation depth of ∼20 nm and ∼28 nm in GaN and AlN, respectively, with an average full width at half maximum for both materials of ∼27 nm. The implantation profiles show that Mn (Fe) dopants in the ternary alloys films are located within a depth 80 nm from the surface, with peak concentrations within the range of ∼20–28 nm set by the binary counterparts.

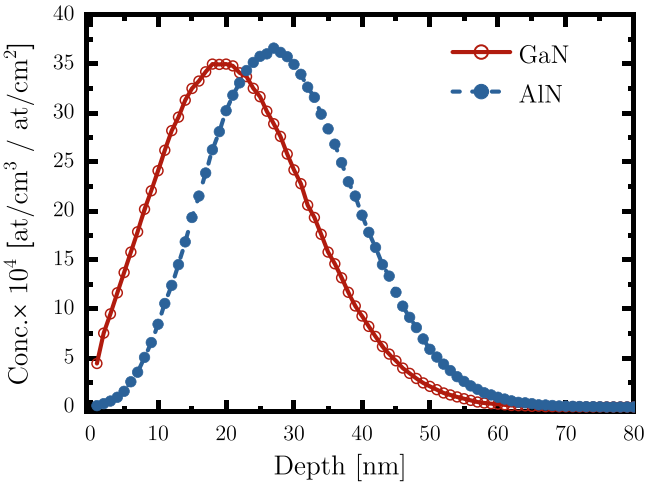

Figure A1. Implantation profiles of ^{57}Mn in AlN and GaN at an angle of 30°.

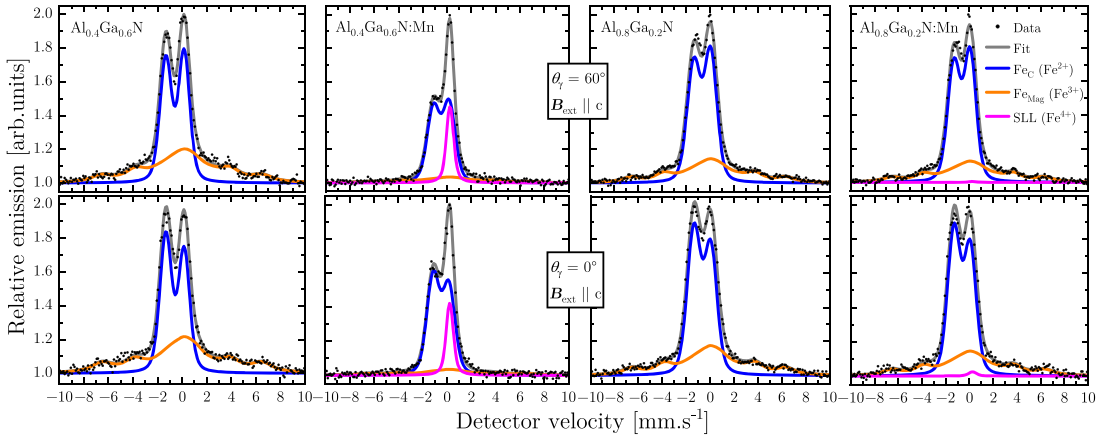

Figure B1. RT ^{57}Fe emission Mössbauer spectra obtained at indicated emission angles after implantation of ^{57}Mn* into $Al_xGa_{1-x}N$ and $Al_xGa_{1-x}N$:Mn for $x = 40\%$ and 80% in an external of $B_{ext} = 0.6$ T.

Appendix B. Additional representative spectra

Selected additional RT emission Mössbauer spectra for $Al_xGa_{1-x}N$ and $Al_xGa_{1-x}N$:Mn for $x = 40\%$ and 80% obtained at the two emission angles is shown in figure B1. The data was analysed using the same fitting procedure and clearly shows the effect of increase in Al concentration on the charge states, mainly the interdependence between the Fe^{3+} and Fe^{4+} shown in figure 4 in the main text and further confirmed by the formation energy dependence obtained DFT calculations as depicted in figure 5.

Appendix C. Notes on DFT calculations

First-principles calculations were performed using a self-consistent Green function method within the DFT [57]. Disorder effects, Al, Mn and Fe impurities in GaN, were simulated using a CPA and an embedded cluster method [62, 63, 69]. Doing this an effective medium was calculated for various concentrations of Al and Mn^{3+} within our CPA method. Fe and Mn impurities of various valencies were then embedded into the effective medium within the real-space embedded cluster method. The valency of Mn and Fe impurities were modelled with a self-interaction correction method [59, 60] which describes adequately valencies of TMs in diluted magnetic semiconductors [61]. Exchange parameters were computed using a magnetic force theorem as it is implemented within the multiple scattering theory [70]. As the reference system was chosen a paramagnetic state modelled by a disordered local moment approach [71].

ORCID iDs

Hilary Masenda https://orcid.org/0000-0003-4722-9622
Haraldur Páll Gunnlaugsson https://orcid.org/0000-0002-8958-0245
Rajdeep Adhikari https://orcid.org/0000-0002-1275-5916
Krish Bharuth-Ram https://orcid.org/0000-0001-9721-6374
Deena Naidoo https://orcid.org/0000-0001-7287-4370
Aitana Tarazaga Martín-Luengo https://orcid.org/0000-0002-3078-4649
Iraultza Unzueta https://orcid.org/0000-0003-3506-0954
Roberto Mantovan https://orcid.org/0000-0002-9353-4137
Torben Esmann Mølholt https://orcid.org/0000-0002-4288-0128
Petko Krastev https://orcid.org/0000-0002-3317-0220
Bingcui Qi https://orcid.org/0000-0002-3546-5102
Sveinn Ólafsson https://orcid.org/0000-0002-3104-1142
Arthur Ernst https://orcid.org/0000-0003-4005-6781
Alberta Bonanni https://orcid.org/0000-0003-4425-0346

References

[1] Morkoç H 2009 *Handbook of Nitride Semiconductors and Devices* vol 1 (New York: Wiley)
[2] Gutt R, Passow T, Kunzer M, Pletschen W, Kirste L, Forghani K, Scholz F, Köhler K and Wagner J 2012 *Appl. Phys. Express* **5** 032101
[3] Nakamura S and Chichibu S F 2000 *Introduction to Nitride Semiconductor Blue Lasers and Light Emitting Diodes* (Boca Raton, FL: CRC Press)
[4] Shur M S 1998 *Solid-State Electron.* **42** 2131–8
[5] Baliga B J 2013 *Semicond. Sci. Technol.* **28** 074011
[6] Adachi S 2009 *Properties of Semiconductor Alloys: Group-IV, III–V and II–VI Semiconductors* (New York: Wiley)
[7] Nastasi M and Mayer J W 2006 *Ion Implantation and Synthesis of Materials* (Berlin: Springer)
[8] Rauschenbach B 2000 *Ion Implantation, Isolation and Thermal Processing of GaN and Related Materials* (Amsterdam: Elsevier) pp 193–249
[9] Amano H, Kito M, Hiramatsu K and Akasaki I 1989 *Japan. J. Appl. Phys.* **28** L2112–4
[10] Nakamura S, Mukai T and Senoh M 1992 *Japan. J. Appl. Phys.* **31** 2883–8
[11] Nakamura S, Iwasa N, Senoh M and Mukai T 1992 *Japan. J. Appl. Phys.* **31** 1258–66
[12] Nakamura S 2015 *Rev. Mod. Phys.* **87** 1139
[13] Akasaki I 2015 *Ann. Phys., Lpz.* **527** 311–26
[14] Amano H 2015 *Ann. Phys., Lpz.* **527** 327–33
[15] Kibria M G, Chowdhury F A, Zhao S, AlOtaibi B, Trudeau M L, Guo H and Mi Z 2015 *Nat. Commun.* **6** 6797
[16] McLaughlin D V and Pearce J M 2013 *Metall. Mater. Trans.* A **44** 1947–54
[17] Cai Q *et al* 2021 *Light Sci. Appl.* **10** 2047–7538
[18] Zhang Q, Yin X and Zhao S 2021 *Phys. Status Solidi RRL* **15** 2100090
[19] Bonanni A, Dietl T and Ohno H 2021 *Dilute Magnetic Materials* (Cham: Springer) pp 923–78
[20] Suffczyński J, Grois A, Pacuski W, Golnik A, Gaj J A, Navarro-Quezada A, Faina B, Devillers T and Bonanni A 2011 *Phys. Rev.* B **83** 094421
[21] Bonanni A *et al* 2011 *Phys. Rev.* B **84** 035206
[22] Navarro-Quezada A, Devillers T, Li T and Bonanni A 2012 *Appl. Phys. Lett.* **101** 081911
[23] Gunnlaugsson H P *et al* 2010 *Appl. Phys. Lett.* **97** 142501
[24] Mølholt T E *et al* 2012 *Phys. Scr.* T **148** 014006
[25] Mantovan R *et al* 2015 *Adv. Electron. Mater.* **1** 1400039
[26] Masenda H *et al* 2016 *J. Magn. Magn. Mater.* **401** 1130–8
[27] Fedoseyev V N *et al* 1997 *Nucl. Instrum. Methods Phys. Res.* B **126** 88–91
[28] Devillers T, Tian L, Adhikari R, Capuzzo G and Bonanni A 2015 *Cryst. Growth Des.* **15** 587–92
[29] Rovezzi M, Schlögelhofer W, Devillers T, Szwacki N G, Li T, Adhikari R, Glatzel P and Bonanni A 2015 *Phys. Rev.* B **92** 115308
[30] Ziegler J F, Ziegler M D and Biersack J P 2010 *Nucl. Instrum. Methods Phys. Res.* B **268** 1818–23
[31] Gunnlaugsson H P 2016 *Hyperfine Interact.* **237** 79
[32] Borowski M, Traverse A and Eymery J P 1997 *Nucl. Instrum. Methods Phys. Res.* B **122** 247–52
[33] Wahl U, Vantomme A, Langouche G, Correia J G and Peralta L 2001 *Appl. Phys. Lett.* **78** 3217–9
[34] Liu C, Alves E, Sequeira A D, Franco N, da Silva M F D and Soares J C 2001 *J. Appl. Phys.* **90** 81–6
[35] Talut G, Reuther H, Mücklich A, Eichhorn F and Potzger K 2006 *Appl. Phys. Lett.* **89** 161909
[36] Malguth E, Hoffmann A, Gehlhoff W, Gelhausen O, Phillips M R and Xu X 2006 *Phys. Rev.* B **74** 165202
[37] Talut G, Reuther H, Zhou S, Potzger K, Eichhorn F and Stromberg F 2007 *J. Appl. Phys.* **102** 083909
[38] Bonanni A *et al* 2007 *Phys. Rev.* B **75** 125210
[39] Malguth E, Hoffmann A and Phillips M R 2008 *Phys. Status Solidi* B **245** 455–80
[40] Talut G, Reuther H, Grenzer J, Mücklich A, Shalimov A, Skorupa W and Stromberg F 2010 *Phys. Rev.* B **81** 155212
[41] Dashdorj J, Zvanut M E, Harrison J G, Udwary K and Paskova T 2012 *J. Appl. Phys.* **112** 013712
[42] Wickramaratne D, Shen J X, Dreyer C E, Engel M, Marsman M, Kresse G, Marcinkevičius S, Alkauskas A and Van de Walle C G V 2016 *Appl. Phys. Lett.* **109** 162107
[43] Wickramaratne D, Shen J X, Dreyer C E, Alkauskas A and Van de Walle C G 2019 *Phys. Rev.* B **99** 205202
[44] Mølholt T E *et al* 2010 *Hyperfine Interact.* **197** 89–94
[45] Blume M and Tjon J A 1968 *Phys. Rev.* **165** 446

[46] Gütlich P, Bill E and Trautwein A X 2011 *Mössbauer Spectroscopy and Transition Metal Chemistry: Fundamentals and Applications* (Berlin: Springer)
[47] Heitz R, Thurian P, Loa I, Eckey L, Hoffmann A, Broser I, Pressel K, Meyer B K and Mokhov E N 1995 *Appl. Phys. Lett.* **67** 2822–4
[48] Gunnlaugsson H P and Masenda H 2019 *J. Phys. Chem. Solids* **129** 151–4
[49] Knudsen J 1977 *J. Phys. Chem. Solids* **38** 883–96
[50] Mørup S 2011 *Magnetic Relaxation Phenomena* (Berlin: Springer) pp 201–34
[51] Masenda H *et al* 2010 *Hyperfine Interact.* **198** 15–22
[52] Alves E, Liu C, Waerenborgh J C, da Silva M F D and Soares J C 2001 *Nucl. Instrum. Methods Phys. Res.* B **175–177** 241–5
[53] Pereira L M C, Wahl U, Correia J G, Decoster S, Amorim L M, da Silva M R, Araújo J P and Vantomme A 2012 *Phys. Rev.* B **86** 195202
[54] Pereira L M C, Wahl U, Decoster S, Correia J G, Amorim L M, da Silva M R, Araújo J P and Vantomme A 2011 *Phys. Rev.* B **84** 125204
[55] Rita E, Wahl U, Correia J G, Alves E and Soares J C 2004 *Appl. Phys. Lett.* **85** 4899–901
[56] Abdalla A S, Khan M S, Alameen S, Eisa M H and Aldaghri O 2021 *Z. Nat.forsch.* A **76** 245–51
[57] Hoffmann M, Ernst A, Hergert W, Antonov V N, Adeagbo W A, Geilhufe R M and Ben Hamed H B 2020 *Phys. Status Solidi* B **257** 1900671
[58] Perdew J P and Wang Y 1992 *Phys. Rev.* B **45** 13244–9
[59] Perdew J P and Zunger A 1981 *Phys. Rev.* B **23** 5048–79
[60] Lüders M, Ernst A, Däne M, Szotek Z, Svane A, Ködderitzsch D, Hergert W, Györffy B L and Temmerman W M 2005 *Phys. Rev.* B **71** 205109
[61] Schulthess T C, Temmerman W M, Szotek Z, Butler W H and Malcolm Stocks G M 2005 *Nat. Mater.* **4** 838–44
[62] Soven P 1967 *Phys. Rev.* **156** 809–13
[63] Gyorffy B L 1972 *Phys. Rev.* B **5** 2382–4
[64] Lide D R (ed) 2003 *CRC Handbook of Chemistry and Physics* 84th edn (Boca Raton, FL: CRC Press) p 10:178
[65] Graf T, Goennenwein S T and Brandt M S 2003 *Phys. Status Solidi* B **239** 277–90
[66] Dietl T and Ohno H 2014 *Rev. Mod. Phys.* **86** 187–251
[67] Zhao K *et al* 2013 *Nat. Commun.* **4** 1442
[68] Zhao K, Chen B, Zhao G, Yuan Z, Liu Q, Deng Z, Zhu J and Jin C 2014 *Chin. Sci. Bull.* **59** 2524–7
[69] Zeller R and Dederichs P H 1979 *Phys. Rev. Lett.* **42** 1713–6
[70] Liechtenstein A I, Katsnelson M I, Antropov V P and Gubanov V A 1987 *J. Magn. Magn. Mater.* **67** 65–74
[71] Gyorffy B L, Pindor A J, Staunton J, Stocks G M and Winter H 1985 *J. Phys. F: Met. Phys.* **15** 1337